INFRARED DIODE LASER SPECTROSCOPIC STUDY OF COMBUSTION RELATED KINETICS

A Thesis
Submitted to the Graduate Faculty
of the
North Dakota State University
of Agriculture and Applied Science

By

Erik Lee Janssen

In Partial Fulfillment of the Requirements
for the Degree of
MASTER OF SCIENCE

Major Department
Chemistry and Biochemistry

October 2015

Fargo, North Dakota

North Dakota State University

Graduate School

Title

INFRARED DIODE LASER SPECTROSCOPIC STUDY OF

COMBUSTION RELATED KINETICS

By

Erik Lee Janssen

The Supervisory Committee certifies that this ***disquisition*** complies with North Dakota State University's regulations and meets the accepted standards for the degree of

MASTER OF SCIENCE

SUPERVISORY COMMITTEE:

John F. Hershberger
Chair

Kenton Rodgers

Svetlana Kilina

Benjamin Braaten

Approved:

1/12/16	Gregory Cook
Date	Department Chair

ABSTRACT

In the introduction section background into the subject of combustion chemistry is presented. The topics included are combustion mechanisms, combustion pollutants, and infrared absorption spectroscopy. Chapter two describes experiments that probe the kinetics of the reactions of CN radicals with several small primary alcohols, as well as the product channels of the reaction between the CN radical and methanol. It was found that all studied reactions were fast, and that CN preferentially abstracts the methyl hydrogen from methanol. Chapter three describes a study of the product channels of the reaction of the hydroxymethyl radical with nitric oxide. It was found that the primary product was the adduct, with minor channels yielding isocyanic acid and nitroxyl radicals.

ACKNOWLEDGEMENTS

This work was supported by the Division of Chemical Sciences, Office of Basic Energy Sciences of the Department of Energy, Grant DE-FG03-96ER14645.

TABLE OF CONTENTS

LIST OF TABLES

LIST OF FIGURES

1. INTRODUCTION

1.1. Overview of Combustion Chemistry

Combustion, from a chemical perspective, is a very complicated process. High temperatures permit reactivity unseen in more typical conditions. Numerous reactions compete for the same pool of starting materials and intermediates. Understanding combustion can allow for minimization of pollutant emissions, ergo a thorough understanding of combustion is desirable. In order to build accurate models of combustion, chemists must study reactions one at a time.

Consider the combustion of methane, a major component of natural gas, in air. The overall reaction is

$$CH_4 + 2O_2 \rightarrow CO_2 + 2H_2O \qquad (1.1)$$

However, the mechanism is quite complicated. The most complete mechanism for this reaction is the GRI-mech 3.0 mechanism, which contains 53 chemical species and 325 elementary reactions.[1] Of the 53 chemicals, only 4, methane, oxygen, nitrogen, and argon can be called initial reactants, and carbon dioxide and water are the intended products, leaving 47 intermediates and side products. This indicates the actual complexity of the combustion process. Part of the reason for such complication is the high temperature rendering atmospheric nitrogen a reactive species, as opposed to its typically inert character. 17 species in the GRI-mech 3.0 mechanism contain at least one nitrogen atom. Ergo, the combustion of methane in oxygen would have 30 intermediate species and 219 reactions, less complicated than in a nitrogen containing atmosphere, but still quite complicated for the combustion of the simplest hydrocarbon.

Combustion typically begins with an activating collision leading to homolytic bond cleavage. This generates transient radical species, which can either go back to their original composition through recombination and a deactivating collision, or they can react with another molecule. This begins a chain reaction, as a radical reacting with a non-radical species will conserve the number of radicals. These species will undergo further reactions, creating a chain process until they recombine in a deactivating collision. A simplified mechanism follows:

$$CH_4 + M \rightarrow CH_3 + H + M \quad (1.2)$$

$$O_2 + M \rightarrow 2O + M \quad (1.3)$$

$$O + CH_4 \rightarrow OH + CH_3 \quad (1.4)$$

$$CH_3 + O_2 \rightarrow CH_3O + O \quad (1.5a)$$

$$\rightarrow CHO + H_2O \quad (1.5b)$$

The number of reactants and reactions quickly increases after the beginning, and each reaction has a particular total rate coefficient and, if multiple products are possible, branching ratio.

In order to ensure that models have a basis in reality, some form of empirical data must be used. Only some of the reaction rates in the GRI-mech mechanism are based on direct experimental data; the mechanism was optimized to best fit these reactions; other reactions had their rates adjusted in order to better match experimental data such as measurement species' concentrations in flames. Due to the complexity of actual combustion, flame measurements are not the only effective strategy; instead, when possible, reactions should be examined individually. Observation of many rate coefficients is complicated by the fact that the corresponding reactions involve transient species not found in ambient conditions. Electrical excitation, photolysis, and controlled high temperatures can be used to generate the species not found in ambient conditions. By carefully selecting the reagents in the reaction mixture, side reactions can be minimized,

eliminated, or at least understood, ideally allowing reactions to be studied individually. Once the reaction is initiated, spectroscopic methods, or other detections techniques are typically used to measure reactant or product concentrations. For reactants, it is useful to take time dependant measurements. By observing the decay of the reactants, a total rate coefficient can be computed. If a reaction has more than one product, such as reaction (1.4) the product concentration measurements are needed to determine the branching fractions. For example, consider the reaction of OH with methanol. The primary reaction is the abstraction of a hydrogen atom, but methanol has two distinguishable hydrogen atoms, ergo there are two possible reactions. These two reactions cannot be distinguished kinetically, as both reactions would consume OH radicals and methanol molecules, however, the production of either the CH_2OH radical or the CH_3O radical can be used to confirm the relative yields, and by extension, the relative rate coefficients. These relative rate coefficients can be combined with the total rate coefficient to give the rate coefficients of the individual reactions.

1.2. Combustion Related Pollutants

The biggest class of combustion-related pollutants is soot. Soot formation is still the topic of significant research, though it is believed that it begins with fuel pyrolysis, wherein heat transforms fuel molecules in the absence of sufficient oxidizing species.[2] This process usually yields C_2H_2, benzene, and polycyclic aromatic hydrocarbons, or PAHs; some soot is partially oxidized, leading to soot particles that are essentially pure carbon. These species then collect to form fairly large particles on the nm to μm scale.

Soot has many environmental and health impacts. It is thought to be the second greatest contributor to anthropogenic global warming; both through direct solar absorption and through melting of ice and associated lowering of global albedo. Fine airborne particulates are also liked

to numerous respiratory problems in people, especially those with pre-existing conditions such as asthma.

Due to its environmental and health impacts, removing soot from combustion output is a high priority. Due to its comparatively large size, soot can be mechanically filtered, though the filters do become saturated over time, which leads to reduction of flow through the filter, which in turn leads to backpressure and mechanical problems. This is particularly a problem in diesel engines, as they tend to produce fairly large amounts of soot yet lack the means to easily regenerate a filter or ensure complete oxidation of fuel molecules. Catalytic oxidation is one possibility, and certain catalysts can be used to remove both soot and NO_X simultaneously.[3]

Nitric oxide (NO) and nitrogen dioxide (NO_2), collectively referred to as NO_X are the other major combustion related pollutants, and are most related to the studies of this thesis. There are three major sources of NO_X. The most prominent of these sources is fuel NO_X, which comes from nitrogen atoms within the fuel itself. The second greatest source is the Zel'dovitch, or thermal mechanism, wherein nitrogen from the atmosphere reacts with oxygen to form NO_X.[4] This process only occurs at very high temperatures, usually in excess of 1500 K. The third and smallest source is the Fenimore or prompt mechanism, which is also between atmospheric nitrogen and oxygen, but cannot be explained through the thermal NO_X mechanism.[5] The basic reactions are as follows:

$$N + O_2 \rightarrow NO + O \text{ (Any)} \tag{1.6}$$

$$O + N_2 \rightarrow NO + N \text{ (Thermal)} \tag{1.7}$$

$$N + OH \rightarrow NO + H \text{ (Thermal)} \tag{1.8}$$

$$CH + N_2 \rightarrow HCN + N \text{ (Prompt)} \tag{1.9a}$$

$$\rightarrow NCN + H \text{ (Prompt)} \quad (1.9b)$$

$$CH_2 + N_2 \rightarrow H_2CN + N \text{ (Prompt)} \quad (1.10)$$

The reaction of NO_X with volatile organic compounds is responsible for photochemical smog, their reaction with molecular oxygen yields considerable amounts of tropospheric ozone, and they are a significant contributor to acid rain.[6]

Most methods of NO_X removal utilize their oxidative capabilities. One very common method is reburning, wherein additional hydrocarbon fuel is added after the combustion is complete. The fuel molecules then reduce the NO_X to N_2, while they are oxidized to CO_2 and H_2O. A typical reburning reaction is:

$$CH_3 + NO \rightarrow HCN + H_2O \quad (1.11)$$

There exist other methods, such as Thermal De-NO_X, which utilize other molecules, such as ammonia, in place of hydrocarbons, but the NO_X remains active as an oxidizing agent. The basic mechanism of the Thermal De-NO_X technique is:

$$NH_3 \rightarrow NH_2 \quad (1.12)$$

$$NH_2 + NO \rightarrow N_2 + H_2O \quad (1.13a)$$

$$\rightarrow HN_2 + OH \quad (1.13b)$$

The precise method by which NH_3 is converted to NH_2 is irrelevant. This method is very effective when coupled with reburning, achieving reductions of up to 90%, and can be improved by adding reagents which speed the formation of the initial NH_2 radical.[6] Yet other methods employ other molecules, but they generally employ the oxidizing capabilities of NO_X.

1.3. Experimental Techniques

All studies discussed herein utilize two major experimental techniques, infrared diode laser absorption spectroscopy, and pulsed laser photolysis. Lead salt diodes, operating at cryogenic temperatures, can be used to give tunable, high resolution (0.0003 cm^{-1} linewidth) infrared light. These lasers are tuned in two ways: the coarse tuning is done by altering the temperature at which the diode operates by use of a precise electric heater, the fine tuning is done by changing the amount of current which flows across the diode. This setup can be tuned over 20~50 cm^{-1}, however, there is generally only consistency over 2~5 cm^{-1}, after which there is likely to be a discontinuity in the light produced by the diode. For example, at a given temperature, one current setting may give a certain wavelength, and a very small change in current will result in a comparatively large change in wavelength. When coupled with a detector with ~1μs response time, it also allows for time resolved detection of a large number of small molecules related to combustion chemistry. It also has the advantage that it can be used to quantify absolute concentration. This requires absorption coefficients, cross-sections, or absolute line strengths; these can be measured or taken from a pre-existing database. The HITRAN database was used in the studies discussed herein. Its most recent iteration covers 47 key atmospheric species and their most prevalent isotopologues.[7] Its data includes high resolution line positions and absolute line strengths. For species not included in the HITRAN database, other literature data were used to locate line positions, and calibration curves were built by varying the pressure of the desired species. These curves were then used to determine the pressure, and by extension, number density, of the species in question. Pulsed laser photolysis allows transient species to be generated from comparatively stable precursors at any temperature. It is also very fast, allowing for nigh-instantaneous generation of transient species.

A typical experiment described in the studies which follow could be described as a photolysis-probe experiment. The reagents are introduced manometrically into an absorption cell. The IR probe laser is passed continuously through the mixture. The UV photolysis laser operates in a pulsed fashion. The beams are restricted and made colinear so that their overlap is nearly 100%. Once the beams pass through the cell, they are separated and the IR beam is focused onto the detector. The signal from the detector is sent to an oscilloscope, which is set to record the signal when the photolysis pulse is fired. This allows a transient signal to be observed as the probed molecules are created, before they can react or diffuse out of the beam path. These signals are recorded and sent to a computer for analysis. The extremely high resolution of the probe laser give this experiment a high degree of selectivity. Even though the reagent mixtures include several different molecules, only a single ro-vibrational spectral line of a single species was probed at a time.

Infrared absorption spectroscopy is based in the measure of how much infrared light passes through a given sample. Like all absorption spectroscopy, it is described by the Beer-Lambert Law: $T = \exp(-\sigma n l)$ where T is the transmittance, which equals the intensity of the light which has passed through the sample over the total intensity of the light, σ is the attenuation cross-section, n is the number density of light attenuating species, and l is the path length. Infrared light typically corresponds to the energy separation of vibrational states. However, at high resolutions rotational quantum states are resolved as well. This separates a high resolution infrared spectrum into three branches: the Q branch, which arises from purely vibrational transitions, the P branch, arising from transitions where the end rotational quantum number is lower than the starting quantum number by one, and the R branch, wherein the final rotational quantum number is higher than the initial quantum number by one. The Q branch lines are

spaced very close together, and if the resolution is not sufficiently high, they can appear as a single line, but the P and R branches are significantly further spaced from one another. The selection rule for IR absorption is typically $\Delta J = \pm 1$, ergo the P branch is a decrease of one and the R branch is an increase of one, the number which follows is the initial state of the molecule. For example, the R(4) transition would be a molecule transitioning from the J = 4 to J = 5 in addition to the vibrational transition. Not every molecule has access to the Q branch due to symmetry, and in some molecules odd or even numbered P and R transitions are forbidden. Figure 1 shows the major IR absorption of NO, with the various branches labeled for clarity.

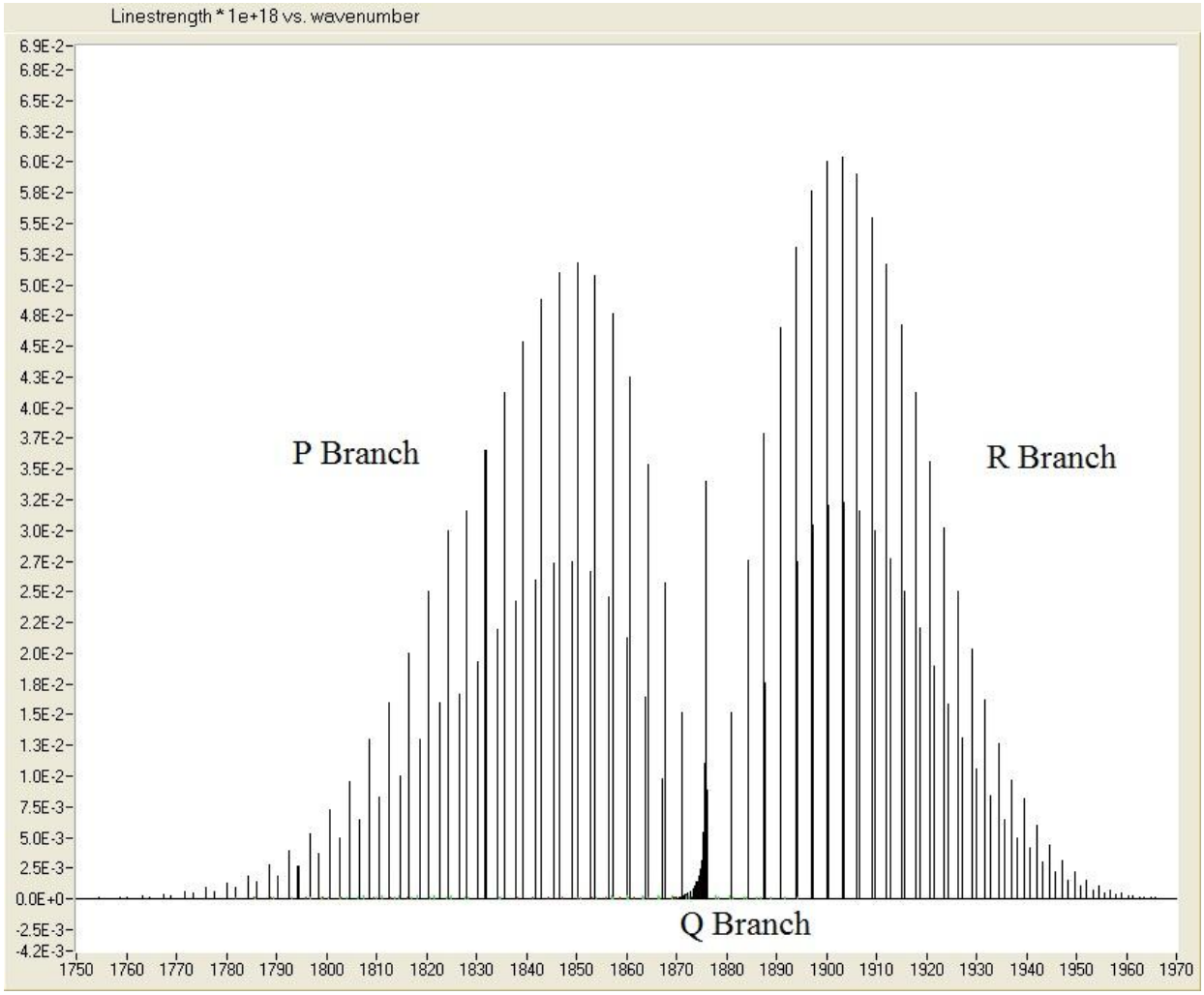

Figure 1: Truncated infrared spectrum of NO with P, Q, and R branches labeled for clarity. Note: a second set of lines in the far IR was omitted to emphasize the branches

In conclusion, a detailed kinetic understanding of NO_X pollutant formation and removal involves many radical-radical and radical-molecule reactions involving a variety of small nitrogen-containing molecules including NO, NH_2, CN, NO_2, etc. The studies reported in this thesis are designed to augment the literature of some of these reactions. The first major study was of the reaction of CN radicals with methanol; this study established both a total rate coefficient as well as a branching ratio between abstraction of an alkyl hydrogen atom vs. the hydroxyl hydrogen atom. The second major study was of the reaction of the CH_2OH radical, the primary product of the previously studied reaction, and NO. In this study we emphasize quantification of product channels.

2. REACTION KINETICS OF THE CN RADICAL WITH PRIMARY ALCOHOLS

2.1. Introduction

The kinetics of the CN radical are of interest due to the role of this molecule in combustion chemistry, especially in relation to formation and removal of NO_x. CN reactions with a variety of molecules have been previously studied, including both saturated and unsaturated hydrocarbons,[8-14] O_2,[8,15-23] NO,[22,24] and NO_2.[23,24] Past work in our laboratory has included study of CN reactions with O_2,[25,26] NO_2,[27] OCS,[28] CS_2,[29] SO_2,[29] and HCNO.[30,31] To date, however, there is no literature on the kinetics of CN reactions with alcohols.

In this study, we report measurements of total rate constants of the reactions of CN with several small primary alcohols:

$$CN + CH_3OH \rightarrow HCN + CH_2OH \quad (2.1a)$$

$$\rightarrow HCN + CH_3O \quad (2.1b)$$

$$CN + CH_3CH_2OH \rightarrow HCN + CH_2CH_2OH \quad (2.2a)$$

$$\rightarrow HCN + CH_3CHOH \quad (2.2b)$$

$$\rightarrow HCN + CH_3CH_2O \quad (2.2c)$$

$$CN + \text{n-propanol} \rightarrow \text{products} \quad (2.3)$$

We also report measurements of HCN and DCN product yields in reactions of CN with partially deuterated methanol in order to determine the competition between channel (2.1a) and (2.1b).

2.2. Experimental

Cyanogen Iodide (ICN) was photolyzed by 266 nm light from the fourth harmonic of an Nd:YAG laser (Continuum Surelite-II):

$$ICN + h\nu\ (266\ nm) \rightarrow CN + I \qquad (2.4)$$

CN radicals and HCN and DCN reaction products were detected by time-resolved infrared diode laser absorption spectroscopy using lead salt diode lasers (Laser Components) operating in the 85 - 110 K region. The infrared beam was collimated by a CaF_2 lens and combined with the UV beam through use of a dichroic mirror. Both beams were restricted to 6 mm in diameter and passed through a 143 cm single pass absorption cell. The beams were separated by a monochromator, and the IR beam was focused onto a 1 mm InSb detection chip (Cincinnati Electronics, ~1μs response time). Transient signals were recorded and signal averaged on a digital oscilloscope, then stored on a computer for analysis. Rate coefficient measurements were taken at 298, 322, 383, and 421 K. Isotope labeled rate coefficient measurements were performed at 298 K. Product yield measurements were taken at 298K. Typical reaction conditions during rate coefficient measurements were P(ICN) = 0.1 Torr, $P(SF_6)$ = 0.5 Torr and variable pressures of the alcohol reagent. Typical reaction conditions in product yield measurements were P(ICN) = 0.1 Torr, $P(CH_3OH)$ = 1.0 Torr, and $P(SF_6)$ = 1.0 Torr. SF_6 was used as a buffer gas in order to quickly relax any nascent vibrationally excited product molecules to a Boltzmann distribution. Average photolysis pulse energy was 7.23 mJ.

ICN (Fluka, 97%) was purified by vacuum sublimation to remove any dissolved gasses. CH_3OH (Sigma-Aldrich, 99.9%), CH_3OD, and CD_3OH (Cambridge Isotope Labs, 99% and 99.5% isotopic purity, respectively) were purified by several freeze-pump-thaw cycles at 77K. CH_3CH_2OH (Sigma-Aldrich, 99.5%) was purified by the same method. n-Propanol

(Sigma-Alrdrich, 99.80%) was purified by several freeze-pump-thaw cycles at 77K. SF_6 (Matheson) was purified by several freeze-pump-thaw cycles at 77K.

The following molecules were probed using IR diode laser absorption spectroscopy:

CN ($v = 1 \leftarrow v = 0$)	R(4) at 2060.804 cm^{-1}
HCN ($v = 1 \leftarrow v = 0$)	P(17) at 3258.442 cm^{-1}
	and P(19) at 3251.823 cm^{-1}
DCN ($v = 1 \leftarrow v = 0$)	R(17) at 2369.42 cm^{-1}
	and R(7) at 2651.107 cm^{-1}

The 1992 HITRAN database was used for locating and identifying spectral lines of HCN. [32] Other published sources were used to locate and identify spectral lines of CN and DCN.[33,34] The transitions used are sufficiently close to the peak of the rotational Boltzmann distributions in order to minimize population changes from any small heating effects due to photolysis laser absorption. Diode output wavelength was confirmed by the use of reference gasses with well known spectra, such as CO or OCS. These spectra were measured by use of a germanium Fabry–Pérot etalon with a well defined fringe spacing, figure 2 shows both the spectrum of OCS and an etalon pattern. A search algorithm was used to select patterns that matched the etalon spacings, however several patterns could match a given set of spacings, therefore human observation and intuition are necessary to assign the wavelength the diode is outputting. Figure 3 shows the stick spectrum as taken from Hunt et al.[35]

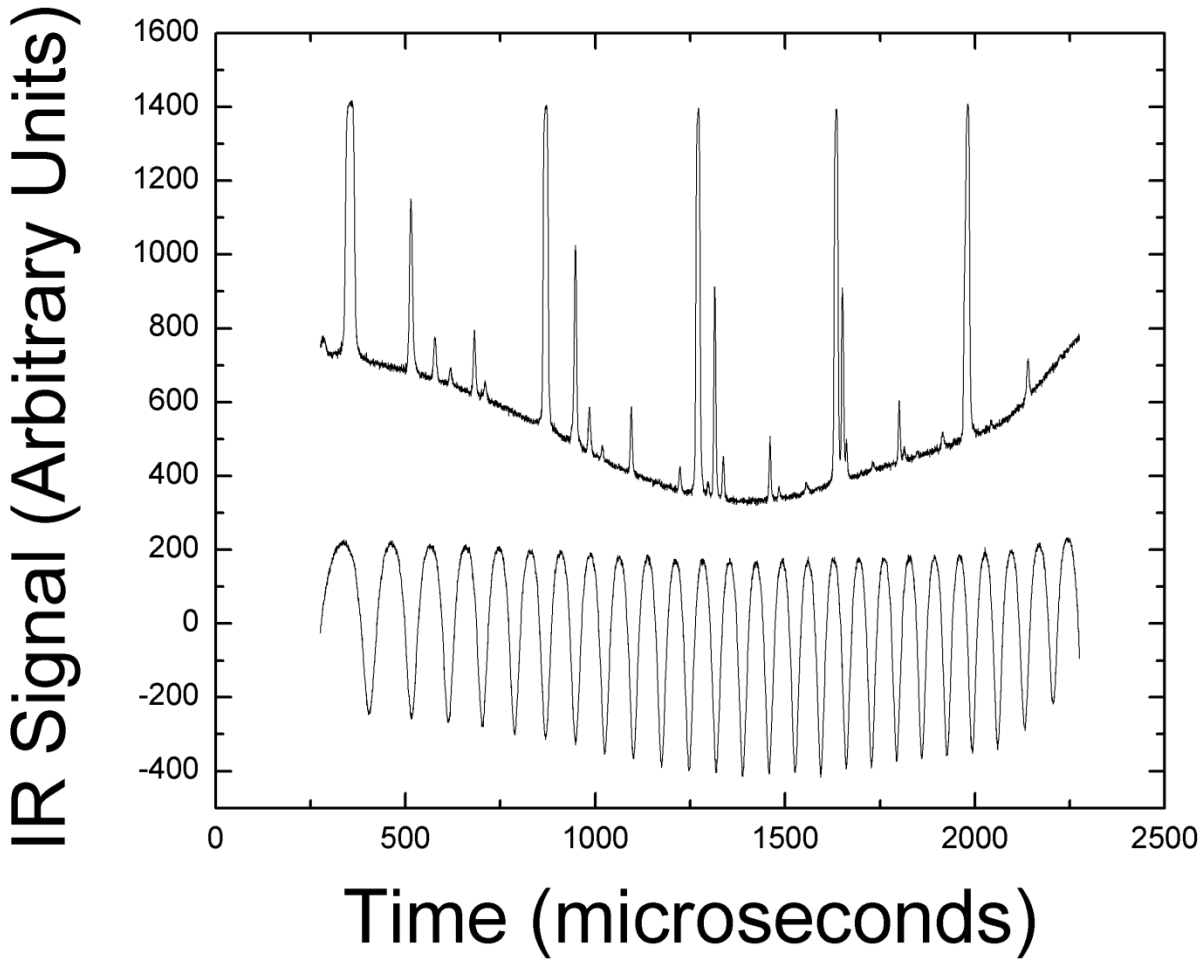

Figure 2: Spectrum of OCS and etalon pattern, upon linear ramp of diode current via modulation. Note that the resulting etalon pattern is nonlinear.

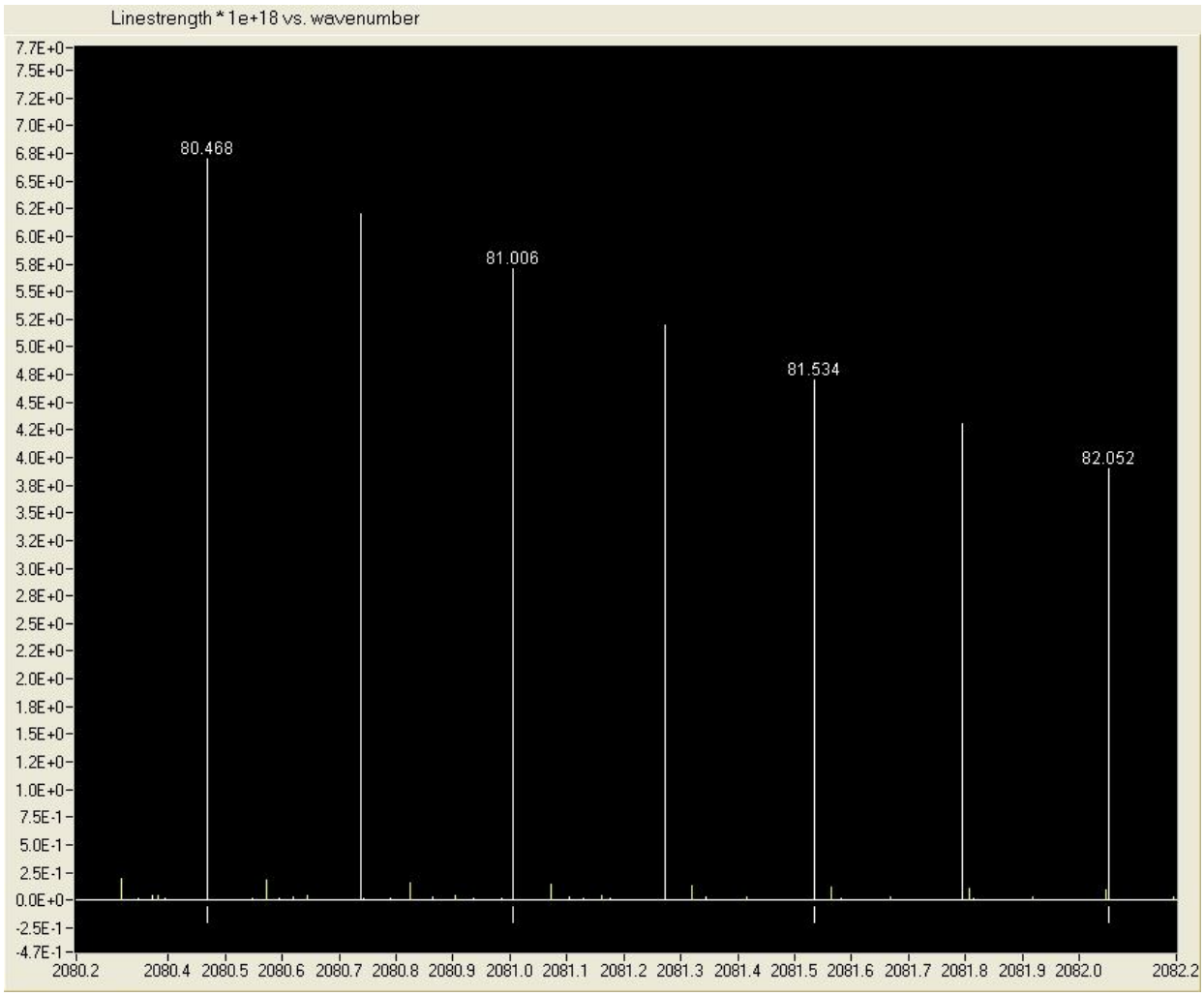

Figure 3: Stick spectrum of OCS. Yellow lines indicate minor isotope lines.

2.3. Results and Discussion

2.3.1. Total Rate Coefficients

The total rate coefficient was measured by diode IR absorption spectroscopy detection of CN radicals. Figure 1 shows typical transient absorption signals obtained with and without added methanol reagent. These signals show a rapid rise in absorption attributed to photolytic formation of CN and rapid relaxation of the nascent hot rotational distribution to a thermal Boltzmann distribution of rotational levels. This occurs on a timescale of <10 μs. Although vibrational relaxation may be much slower, the photolysis of ICN at 248 nm is known to produce primarily

vibrational ground state CN radicals. In the absence of methanol, the observed decay rate of CN radicals was approximately ~25 ms^{-1} over a 160 μs observation window. This non-zero decay is attributed to reactions other that the title reaction (primarily CN + CN self reaction, reaction with trace O_2 impurities, and diffusion of CN molecules out of the probed region). The decay rate increased to about 75 ms^{-1} upon addition of 0.1 Torr of CH_3OH. Typical CN radical densities were approximately 2.0×10^{13} molecules/cm^3. Under these conditions, pseudo-first order conditions will be expected if the concentration of CH_3OH is greater than ~4×10^{14} molecules/cm^3 = 12 mTorr. Therefore, the time-dependent CN concentration may be described according to a standard pseudo-first order kinetics treatment:

$$[CN]_t = [CN]_0 \exp(-k't) \tag{2.5}$$

$$k' = k_1 [CH_3OH] + k_0 \tag{2.6}$$

Where k' is the observed pseudo-first order CN signal decay, k_1 is the desired bimolecular rate coefficient, and k_0 is the pseudo-first order decay in the absence of methanol reagent. Transient signals were fit to the above function to give k' values, which were then plotted as a function of $[CH_3OH]$. A typical plot is shown in Figure 2. The slope of this plot is the desired bimolecular rate coefficient, k_1.

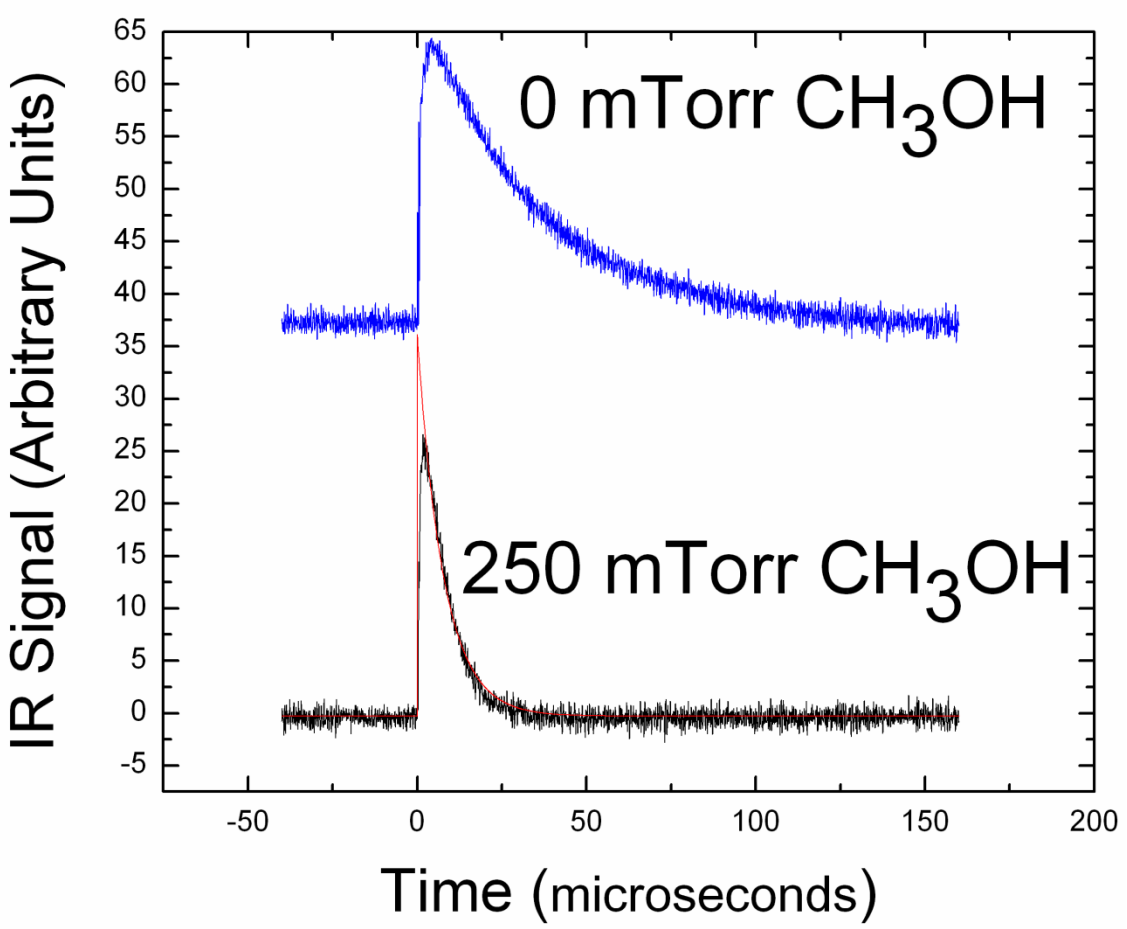

Figure 4: Infrared absorption transient signals, detecting [CN] vs. time. Upper trace: without added alcohol reagent. Lower trace: with 250 mTorr of CH_3OH reagent. Red line over lower trace: single exponential decay fit. Typical reaction conditions (both traces): P(ICN) = 0.10 Torr, $P(SF_6)$ = 0.50 Torr.

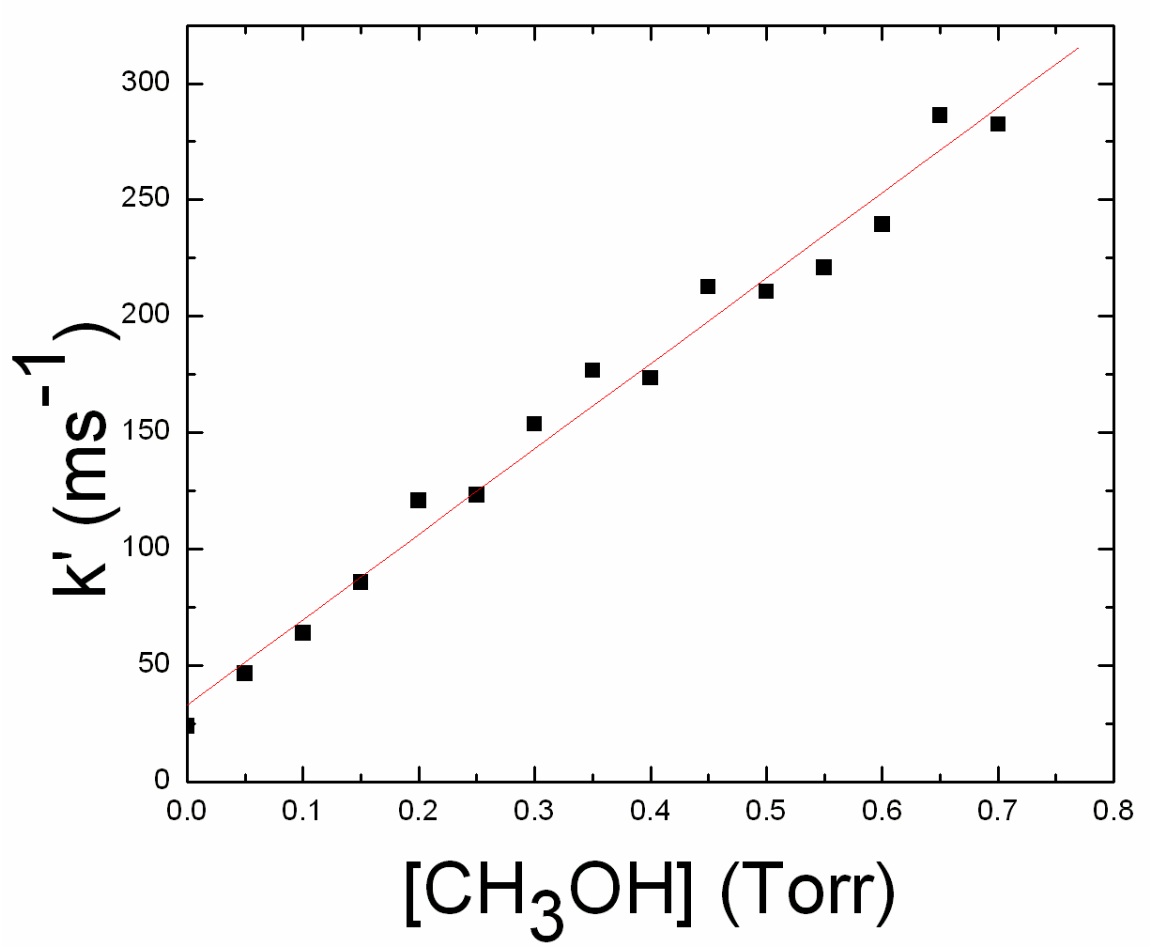

Figure 5: Plot of pseudo-first-order decay rate vs. pressure of CH_3OH.

Rate coefficients of the CN + CH_3OH reaction were determined over the temperature range (298 – 421 K). Figure 3 shows an Arrhenius plot of the data. Only a slight temperature dependence was observed, resulting in a large amount of relative scatter in this plot. From the slope and intercept, we obtain the expression:

$$k_1(T) = (2.16 \pm 0.46) \times 10^{-11} \exp[(-214 \pm 76)/T] \text{ cm}^3 \text{ molec}^{-1} \text{ s}^{-1} \quad (2.7)$$

From this equation the activation energy was determined to be 1.78 ± 0.63 kJ mol^{-1}.

In addition, rate constant measurements at 298 K were performed for reactions of CN with ethanol and n-propanol. The results are shown in Table 1.

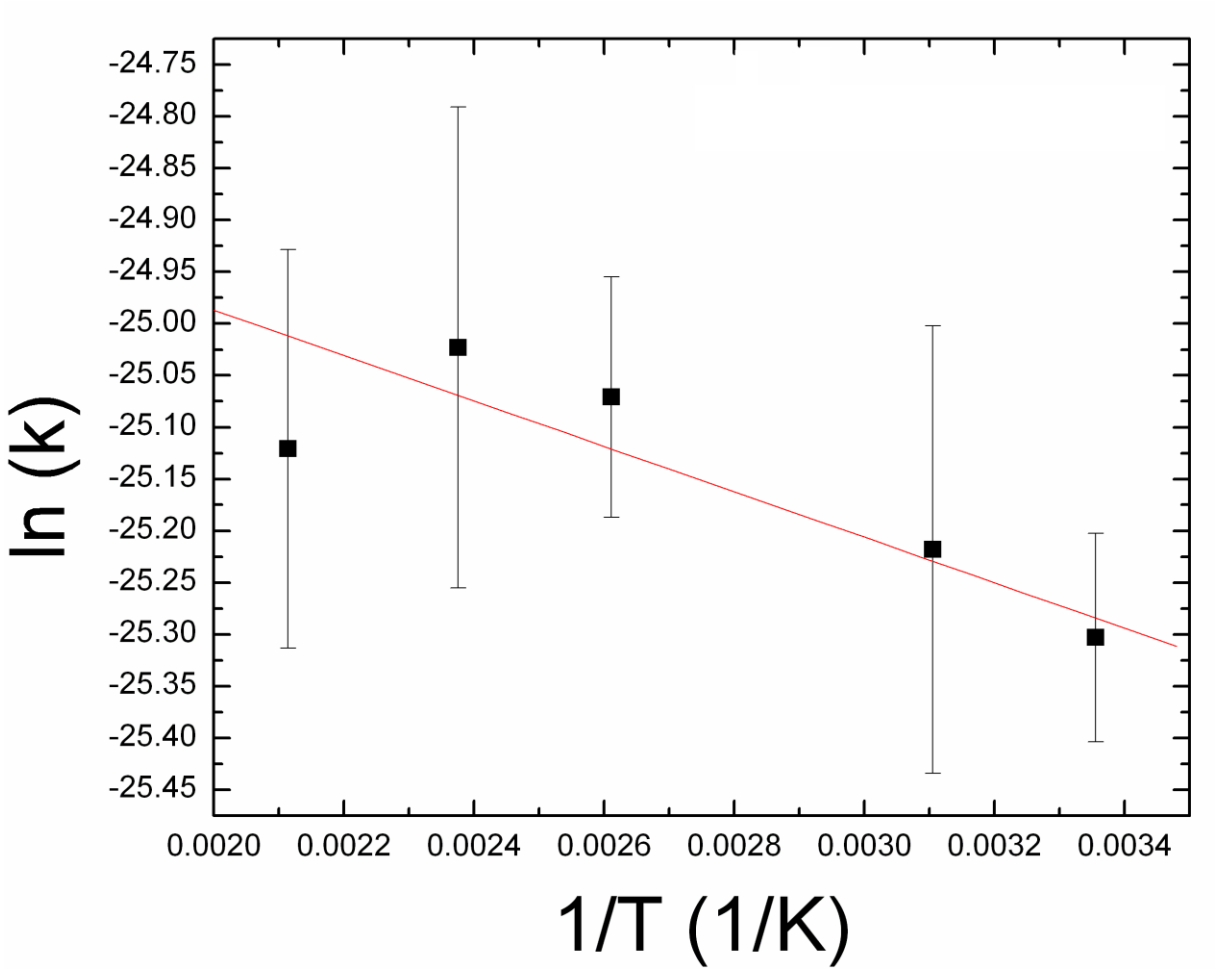

Figure 6: Arrhenius plot of rate constant of the CN + CH_3OH reaction.

Table 1: Rate coefficient vs. temperature and uncertainties.

Temperature (K)	Rate Coefficient (cm^3 $molecule^{-1}$ s^{-1})	Uncertainty (1 standard deviation)
298	1.03×10^{-11}	1.02×10^{-12}
322	1.14×10^{-11}	2.58×10^{-12}
383	1.30×10^{-11}	1.56×10^{-12}
421	1.39×10^{-11}	3.34×10^{-12}
473	1.25×10^{-11}	2.47×10^{-12}

Table 2: Rate coefficients of CN + alcohol reactions.

Reaction	Bimolecular Rate Coefficient (298K) (cm^3 $molecule^{-1}$ s^{-1})
CN + CH_3OH	$(1.03 \pm 0.10) \times 10^{-11}$
CN + CH_3OD	$(1.19 \pm 0.09) \times 10^{-11}$
CN + CD_3OH	$(9.05 \pm 0.32) \times 10^{-12}$
CN + C_2H_5OH	$(2.84 \pm 0.78) \times 10^{-11}$
CN + n-propanol	$(7.57 \pm 1.45) \times 10^{-11}$

2.3.2. Product Yields

Infrared diode laser absorption spectroscopy was used to detect HCN and DCN products of the reactions of CN with CH_3OH, CD_3OH, and CH_3OD. In addition to reactions (2.1a) and (2.1b), above, the following reactions can occur when partially deuterated reagents are used:

$$CN + CD_3OH \rightarrow DCN + CD_2OH \quad (2.8a)$$

$$\rightarrow HCN + CD_3O \quad (2.8b)$$

$$CN + CH_3OD \rightarrow HCN + CH_2OD \quad (2.9a)$$

$$\rightarrow DCN + CH_3O \quad (2.9b)$$

All detection experiments were performed at 298 K. Figure 4 shows a typical HCN product transient signal for the reactions of CN with CH_3OH and CD_3OH. These signals were converted to absolute concentrations of HCN using known linestrengths from the HITRAN database, as described in previous publications.[25] Typical concentrations obtained under our experimental conditions were ~1.92×10^{13} molecule cm^{-3}. In principle, if channels (2.1a) and (2.1b) are the only products of reaction (2.1), and if the CH_3OH concentration is sufficient to ensure that all CN radicals react with CH_3OH, then the HCN yield should be equal to the initial $[CN]_0$ produced in the photolysis. In practice, we find that with 1.00 Torr of CH_3OH, the HCN yield is

typically only about ~80% of $[CN]_0$, suggesting that other pathways for CN removal exist; the intercepts apparent in Figure 2 are in qualitative agreement with this. In addition, however, the calculation of $[CN]_0$ from the UV cross section of ICN and the photolysis laser pulse energy has a significant uncertainty of ~15-20%. Therefore, in order to normalize the HCN yields, the HCN yield in the following reaction was measured:

$$CN + C_6H_{12}\ (\text{cyclohexane}) \rightarrow HCN + C_6H_{11} \qquad (2.10)$$

Because this reaction is expected to form HCN in 100% yield, this provides a useful comparison. The resulting HCN number densities are shown in Table 2.

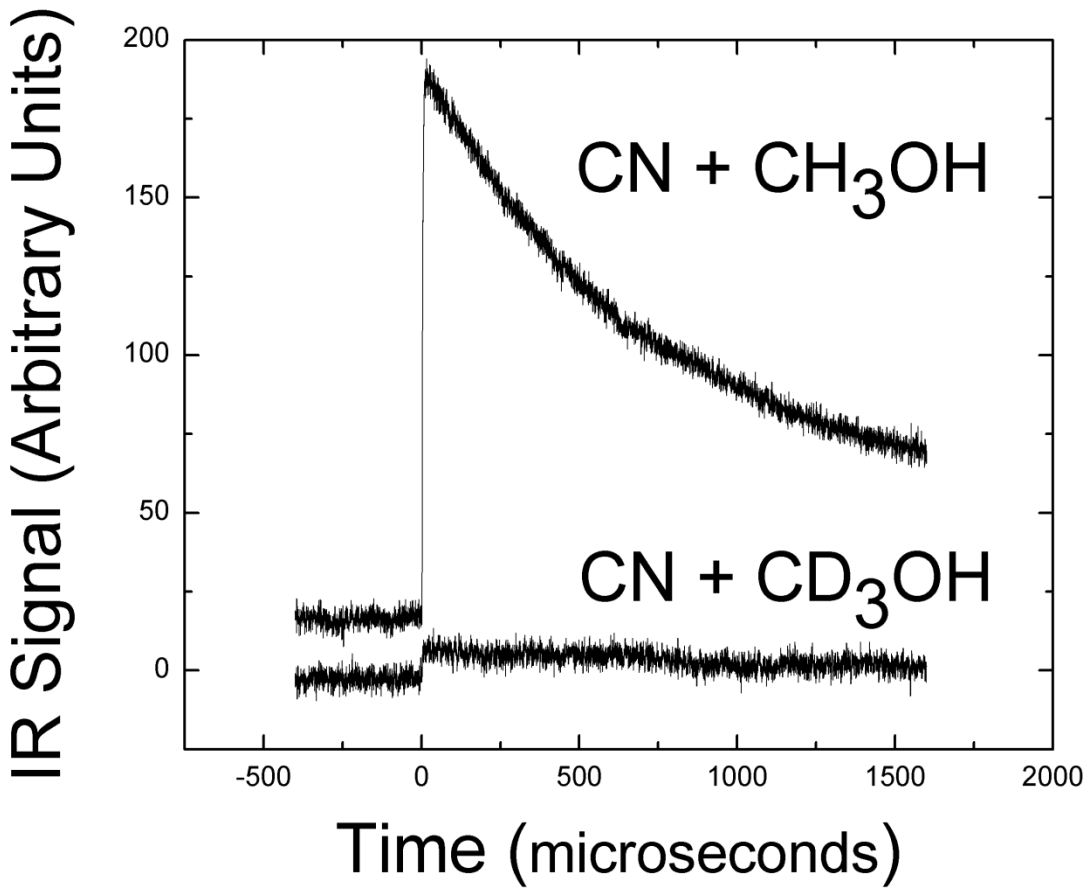

Figure 7: Transient infrared absorption signals for HCN product detection from the CN + CH_3OH and CN + CD_3OH reactions. Typical reaction conditions: P(ICN) = 0.10 Torr, P(CH_3OH) = 1.00 Torr (upper trace only), P(CD_3OH) = 1.00 Torr (lower trace only), P(SF_6) = 1.00 Torr.

Table 3: HCN yields of CN reactions.

Reaction	Absolute Number Density (molecule cm^{-3})	Normalized Number Density
CN + C_6H_{12}	$(2.08 \pm 0.77) \times 10^{13}$	1.00 ± 0.37
CN + CH_3OH	$(1.92 \pm 0.86) \times 10^{13}$	0.92 ± 0.41
CN + CD_3OH	$(0.165 \pm 0.124) \times 10^{13}$	0.08 ± 0.06
CN + CH_3OD	$(1.55 \pm 0.52) \times 10^{13}$	0.74 ± 0.25

Several conclusions may be obtained from the data. Firstly, the HCN yield of reaction (2.1) is approximately the same within experimental uncertainty as that of the reference reaction (2.10). This suggests that HCN forming channels, i.e. (2.1a) and (2.1b), do indeed dominate

reaction (2.1), involving nondeuterated reagents. The HCN yield of reaction (2.8), however, is approximately an order of magnitude smaller. This indicates, that channel (2.8b), abstraction of the hydroxyl hydrogen, is only a minor channel. The HCN yield of reaction (2.9) is close but slightly smaller than that of reaction (2.1), indicating that abstraction of the methyl hydrogen dominates. This result is not unexpected, as similar reactivity has been demonstrated in previous studies of Cl+CH_3OH kinetics.[36] We note that the isotopic purity of the deuterated samples is ~99%. A 1% impurity of CH_3OH in the CD_3OH sample would be insufficient to produce the observed HCN yields. We therefore conclude that while the expected alkyl abstraction channel dominates, a small but measurable yield of ~8% into the hydroxyl channel (2.4b) is observed.

DCN yields were also measured in a similar fashion, except that C_2D_6 rather than C_6H_{12} was used as the reference reaction. Because we do not have linestrengths for DCN spectral transitions, we only measured relative yields, relative to the CN + C_2D_6 reference reaction. The results are shown in Table 3. We find large amount of DCN formed in reaction (2.8), as expected if the alkyl abstraction channel (2.8a) dominates. We were able to detect only a very small DCN yield in reaction (2.9), suggesting that channel (2.9b) is very small.

Table 4: DCN yields of CN reactions.

Reaction	Normalized Number Density
CN + C_2D_6	1.00 ± 0.38
CN + CD_3OH	0.93 ± 0.14
CN + CH_3OD	0.02 ± 0.01

2.4. Conclusions

Reactions of CN with CH_3OH and partially deuterated analogues as well as higher primary alcohols were studied by infrared absorption spectroscopy. All of the probed reactions are fast, with rate constants increasing with alkyl chain length. Only very small isotope effects are observed in the total rate constants. HCN/DCN product detection experiments in the CN + methanol reaction demonstrate that abstraction from alkyl hydrogen or deuterium dominates, but a minor channel (~8%) involving attack at the hydroxyl hydrogen is also observable. This reaction therefore represents a fairly clean route to producing the hydroxymethyl radical, CH_2OH.

3. BRANCHING RATIOS OF THE REACTION OF THE HYDROXYMETHYL RADICAL WITH NITRIC OXIDE

3.1. Introduction

The hydroxymethyl (CH_2OH) radical is of interest to combustion chemists due to its importance in the combustion and atmospheric chemistry, as well as its capability to react with NO_X species. Reactions of the CH_2OH radical with NO_2,[37,38] O_2,[39] hydrogen halides,[40-43] H_2O,[44] H_2O_2,[45] certain saturated and unsaturated hydrocarbons and hydrocarbon radicals,[46-49] OH Radicals,[46] and HO_2 radicals have been studied by experiment or ab initio calculation.[46,50] In the one previous study of the kinetics of the title reaction, Pagsberg et al suggested two possible product channels:[37]

$$CH_2OH + NO + M \rightarrow HOCH_2NO \quad (3.1a)$$

$$CH_2OH + NO \rightarrow CH_2O + HNO \quad (3.1b)$$

They used pulse radiolysis to generate F atoms, followed by the $F + CH_3OH$ reaction to generate CH_2OH radicals. Detection of CH_2OH by UV absorption spectroscopy yielded a total rate constant of 2.5×10^{-11} cm^3 $molecule^{-1}$ s^{-1} at room temperature and 1 atm total pressure. Based on the UV absorption spectra obtained, they suggested that adduct formation may dominate the reaction, but were unable to estimate the yield of any possible bimolecular product channels. Furthermore, there are several additional bimolecular channels that are thermodynamically possible. A more complete set of product channels is

$$CH_2OH + NO + M \rightarrow HOCH_2NO \quad (3.1a)$$

$$CH_2OH + NO \rightarrow CH_2O + HNO \quad \Delta H^0_{298} = -90.0 \text{ kJ/mol} \quad (3.1b)$$

$$\rightarrow HCN + H_2O_2 \qquad \Delta H^0_{298} = -74.7 \text{ kJ/mol} \quad (3.1c)$$

$$\rightarrow HNCO + H_2O \qquad \Delta H^0_{298} = -431 \text{ kJ/mol} \quad (3.1d)$$

$$\rightarrow HCNO + H_2O \qquad \Delta H^0_{298} = -142 \text{ kJ/mol} \quad (3.1e)$$

$$\rightarrow HCO + H_2NO \qquad \Delta H^0_{298} = 44.6 \text{ kJ/mol} \quad (3.1f)$$

$$\rightarrow NCO + OH + H_2 \qquad \Delta H^0_{298} = 167 \text{ kJ/mol} \quad (3.1g)$$

Where the thermodynamic data are obtained from the NIST-JANAF standard tables,[51] other published sources for HNCO, HCNO, HNO,[52] H_2NO,[53] and CH_2OH.[54] No thermochemical data were available for the adduct formation channel.

In this paper, we report infrared absorption measurements of the yield of product channels of the title reaction. The experimental approach used in this study is to photolytically produce CN radicals, followed by the CN + CH_2OH reaction:

$$ICN + h\nu \text{ (266 nm)} \rightarrow I + CN \quad (3.2)$$

$$CN + CH_3OH \rightarrow HCN + CH_2OH \quad (3.3a)$$

$$\rightarrow HCN + CH_3O \quad (3.3b)$$

The kinetics of reaction (3.3) have been reported in a previous publication in our laboratory [19]. It is fast, with $k_3 = 2.5 \times 10^{-11}$ cm^3 $molecule^{-1}$ s^{-1} at 298 K. A key point is that channel (3a) was shown to be the dominant product channel, with an estimated yield of $\varphi_{3a} = 0.94$, with only very small amounts (0.08) of channel (3b). This approach therefore represents a relatively clean route to hydroxymethyl radicals.

3.2. Experimental

The experimental apparatus was described in the previous chapter. The photolysis laser was an Nd:YAG laser (Continuum Surelite-II) operating on the fourth harmonic. Typical reaction mixtures included ICN (0.10 Torr), CH_3OH (1.0 Torr), NO (variable pressure), and SF_6 buffer gas (1.0 Torr). Reaction products were detected by time-resolved infrared absorption spectroscopy using high resolution lead salt diode lasers (Laser Components). The UV and IR beams were copropagated through a 143 cm single pass absorption cell. The beams were then separated by a ¼-m monochromator and the infrared light was detected on a 1 mm InSb detector (Cincinnati Electronics, ~1 μs response time). Transient signals were collected and signal averaged by a digital oscilloscope and stored on a computer. All measurements were taken at 298 K.

ICN (Fluka, 97%) was purified by vacuum sublimation to remove dissolved gasses. CH_3OH (Sigma-Aldrich, 99.9%), CH_3OD, and CD_3OH (Cambridge Isotope Labs, 99% and 99.5% isotopic purity, respectively) were purified by several freeze-pump-thaw cycles at 77 K. NO (Matheson) was purified by freezing NO_2 impurities at 173 K, then collecting the NO in a sealed liquid nitrogen trap, followed by several freeze-pump-thaw cycles. SF_6 (Matheson) was purified by several freeze-pump-thaw cycles.

HNCO samples (used for calibration purposes only) were synthesized as described by Fischer, et al, substituting sodium cyanate for potassium cyanate.[55] HCNO samples were synthesized as described by Feng.[56]

The following molecules were probed using infrared diode laser absorption spectroscopy:

$HCN(v = 1 \leftarrow v = 0)$ P(19) at 3251.823 cm^{-1}

$HNO(v = 1 \leftarrow v = 0)$ at 2669.8907 cm^{-1}

HNCO($\nu = 1 \leftarrow \nu = 0$)	R(15) at 2280.0663 cm^{-1}
HCNO($\nu = 1 \leftarrow \nu = 0$)	R(10) at 2203.851 cm^{-1}
CO($\nu = 1 \leftarrow \nu = 0$)	R(2) at 2154.59 cm^{-1}
H_2O($\nu = 1 \leftarrow \nu = 0$)	5 3 3 at 1895.19727 cm^{-1}
H_2CO($\nu = 1 \leftarrow \nu = 0$)	5 1 5 at 2796.32910 cm^{-1}
N_2O($\nu = 1 \leftarrow \nu = 0$)	P23 at 2202.74438 cm^{-1}

Transient signals were collected both on and off resonance with the listed spectral lines. Off resonance signals, which are attributed to thermal deflection effects, were subtracted from the on resonance signals in order to obtain absorption profiles for the relevant molecules.

The HITRAN database was used for locating and identifying HCN, CO, H_2O, and H_2CO lines. Other published sources were used to locate and identify HNO,[57] HNCO,[58] and HCNO lines.[59]

3.3. Results and Discussion

3.3.1. Product Yields

Of the list of probed species described above, three product molecules were detected by transient infrared absorption spectroscopy. Figure 1 shows transient signals for HNCO and HNO molecules; these molecules were detected only if all three reagents (ICN, CH_3OH, and NO) were present. Additionally, HCN was detected both with and without NO reagent, as shown in Figure 6. Transient signals for the other species listed above were negligible, but upper limits to detectable signals were estimated when possible. The signals displayed fast rises in the first few microseconds, attributed for rapid formation of the detected product molecules, as well as relaxation of any ro-vibrational excited state populations to a Boltzmann distribution (the SF_6

buffer gas is included to speed up this relaxation). This is typically followed by a slow decay, which for stable species is dominated by diffusional loss of the detected molecule out of the probed volume. The somewhat faster decay in the lower trace of Figure 6 is consistent with this interpretation, as diffusion is faster at the lower total pressure of 2.1 Torr, compared to the higher pressure of 3.1 Torr used in the upper trace.

Peak-peak amplitudes were converted to absolute concentration using known line strengths from the HITRAN database for HCN, CO, and N_2O. Calibration of HNCO signals was accomplished by filling the cell with varying pressures of HNCO and measuring static absorption signals. The natural logarithms of the signals were then plotted to create a Beer-Lambert plot. This plot is shown in Figure 8. The slope of the line in this plot, divided by the length of the absorption cell, yields the absorption coefficient of the molecule in question. The absorption coefficient obtained for the R(15) line of HNCO at 2280.0663 $cm^{-1}$was 1.38 cm^{-1} $Torr^{-1}$ (base e).

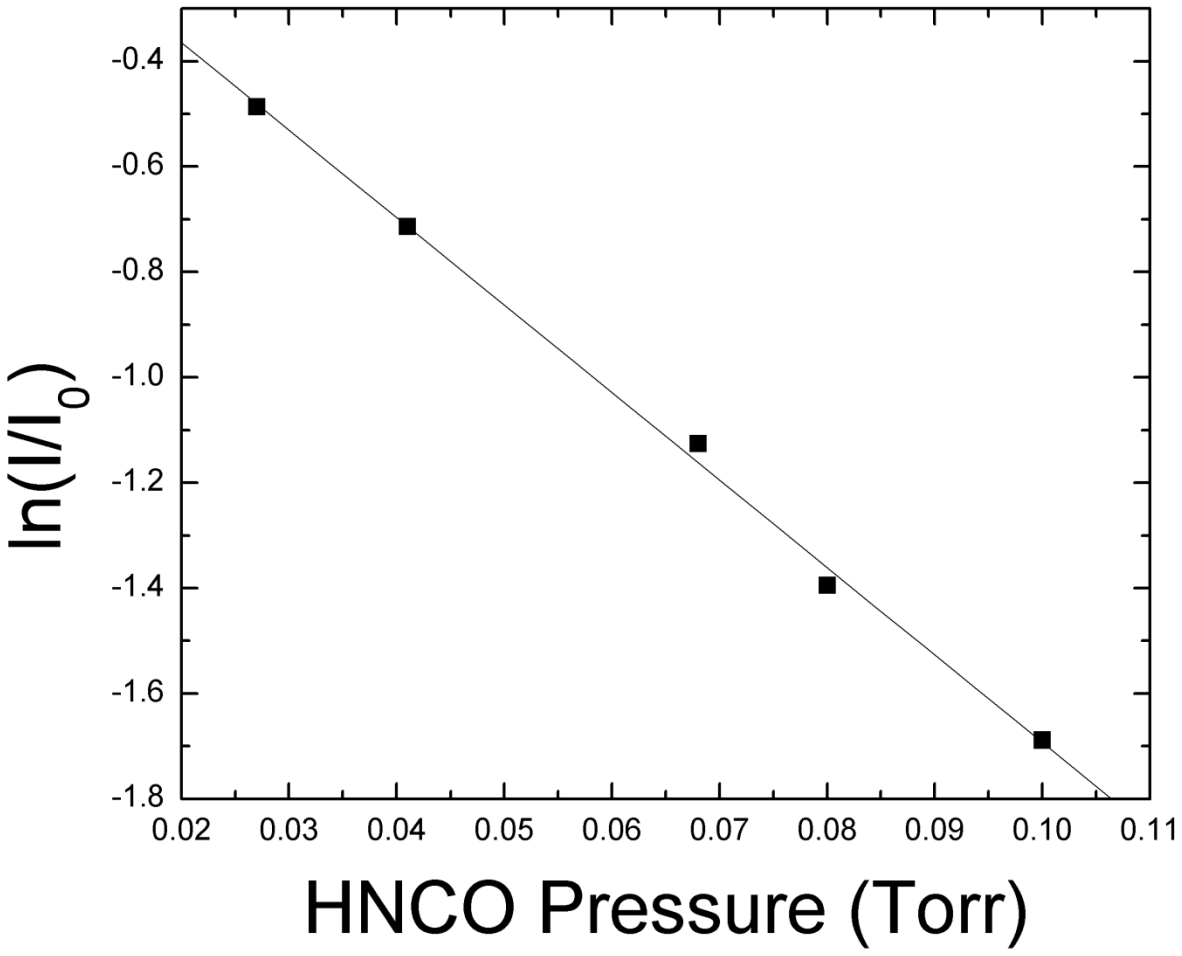

Figure 8: Beer-Lambert plot for HNCO in a 12 cm single-pass absorption cell.

A similar procedure was used to calibrate HCNO (resulting in 1.94 cm^{-1} $Torr^{-1}$ for the R(10) line at 2203.851 cm^{-1}), and CH_2O (resulting in 0.196 cm^{-1} $Torr^{-1}$ for the line at 2796.32910 cm^{-1}).

HNO was calibrated by the following reaction sequence:

$$ICN + h\nu\ (266) \rightarrow I + CN \quad (3.4)$$

$$CN + CH_2O \rightarrow HCN + HCO \quad (3.5)$$

$$HCO + NO \rightarrow HNO + CO \quad (3.6)$$

(Note that CN does not react quickly with NO at low pressures). By measuring the photolysis laser pulse energy, the number density of CN radicals was estimated. In the limit of high CH_2O and NO concentrations, this reaction sequence converts most CN radicals to HNO. Detection of the resulting transient signal for HNO then provides the calibration, leading to 0.069 cm^{-1} $Torr^{-1}$ for the HNO line at 2669.8907 cm^{-1}.

As shown in Figure 9, significant amounts of HNCO as well as small amounts of HNO are produced in this reaction. Figure 10 shows that significant amounts of HCN are produced, but with essentially identical yields with and without the NO reagent. This is attributed to the production of HCN in reaction (3.3), and indicates that production of HCN via channel (3.1c) of the title reaction is small or insignificant.

Figure 11 shows the number density of HNCO produced as a function of NO reagent pressure. At low NO pressures, reaction (3.1) competes with other CH_2OH loss mechanisms such as reaction with trace O_2, diffusional losses, etc. In the limit of high NO and CH_3OH pressures, most CN radicals produced in the photolysis are converted to CH_2OH in reaction (3a), and most CH_2OH radicals react with NO. As shown, this high pressure limit is reached at pressures above approximately 0.5 Torr.

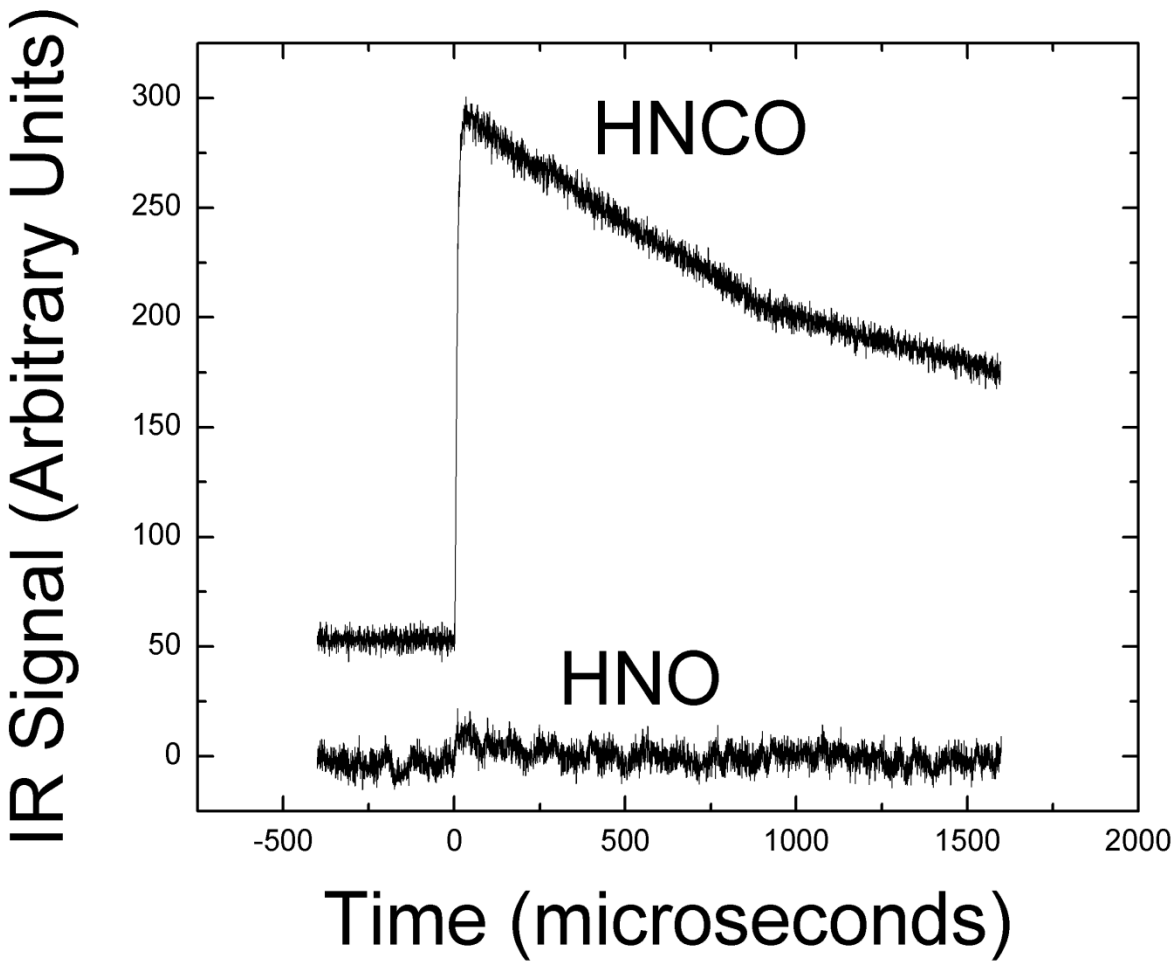

Figure 9: Typical transient signals for HNCO and HNO product molecules. Typical reaction conditions: P(ICN) = 0.1 Torr, P(CH_2OH) = 1.0 Torr, P(NO) = 1.0 Torr, P(SF_6) = 1.0 Torr.

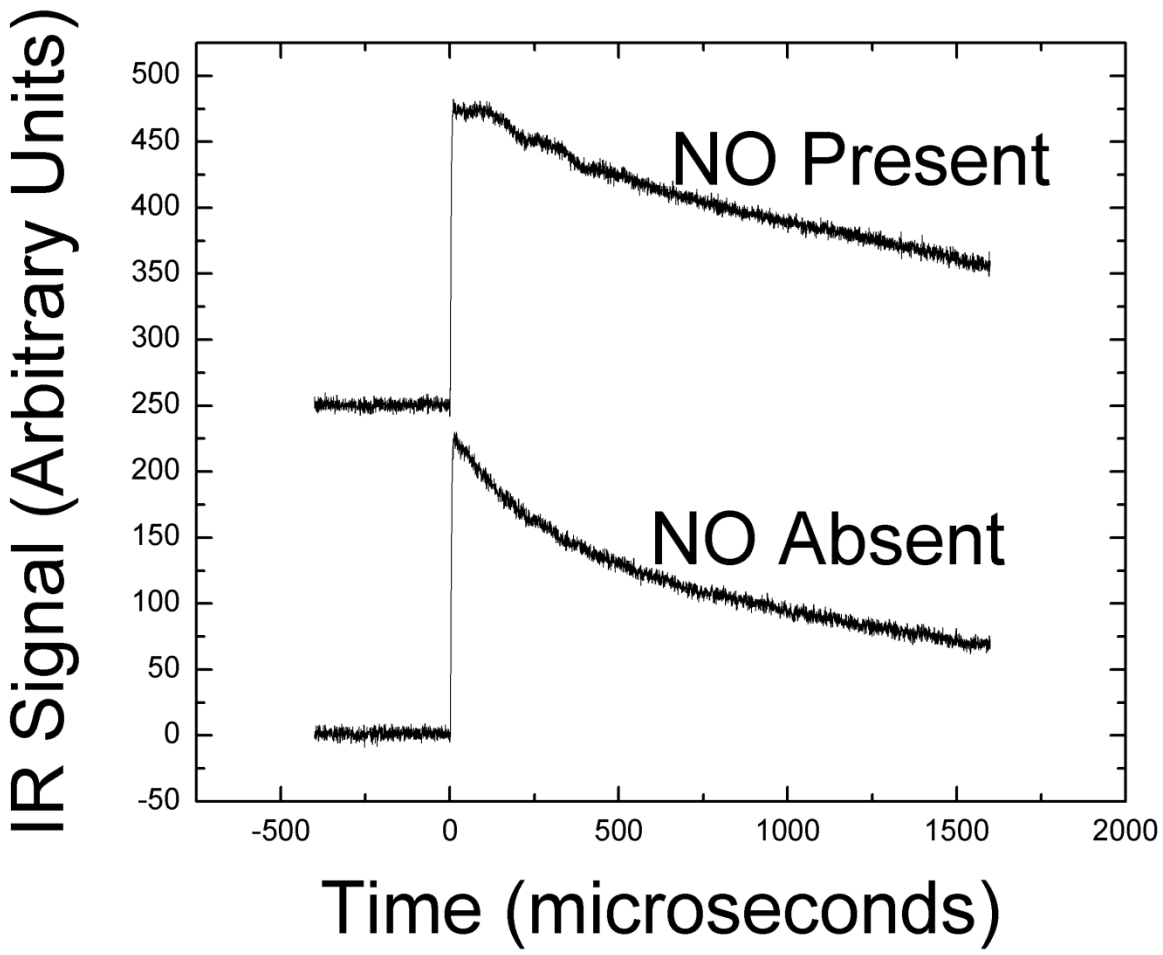

Figure 10: HCN yields in the presence and absence of NO. Typical reaction conditions: P(ICN) = 0.1 Torr, P(CH_3OH) = 1.0 Torr, P(NO) = 0 or 1.0 Torr, and P(SF_6) = 1.0 Torr.

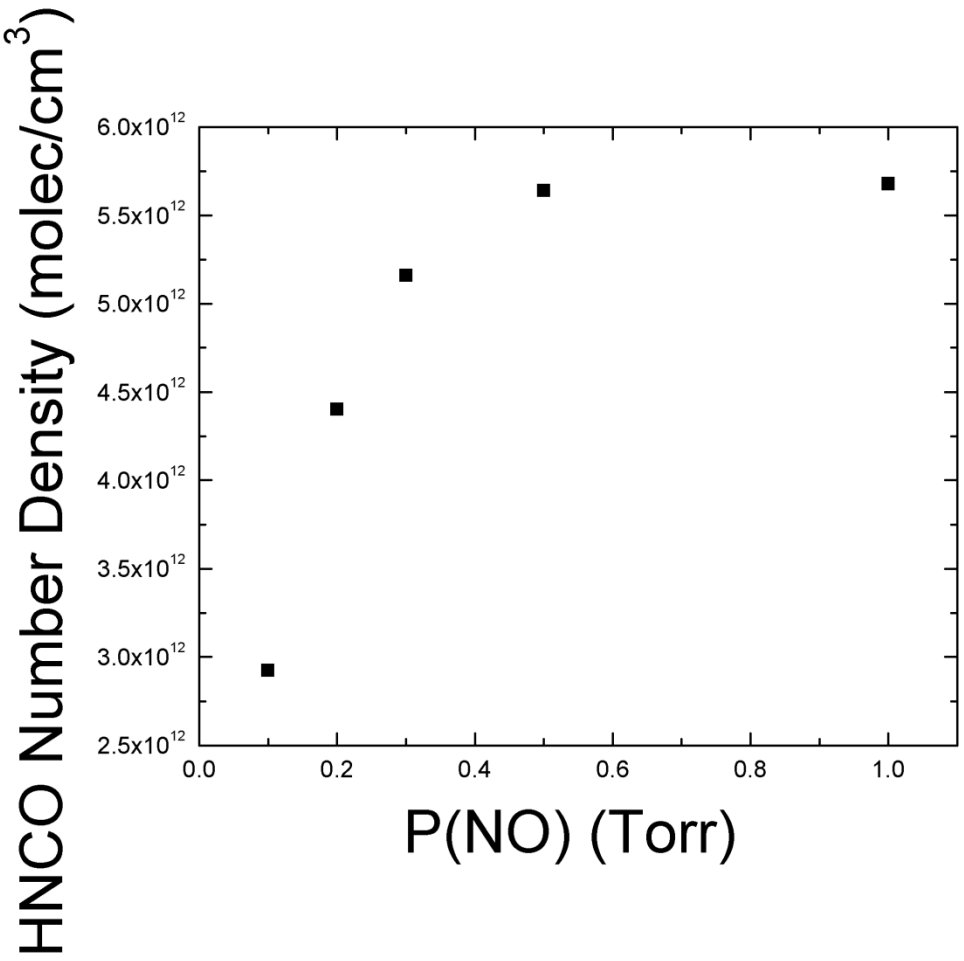

Figure 11: HNCO yield vs. NO pressure. Typical reaction conditions: P(ICN) = 0.1 Torr, $P(CH_2OH)$ = 1.0 Torr, P(NO) = variable, $P(SF_6)$ = 1.0 Torr.

The resulting product yields for detected product molecules as well as estimated upper limits of undetected molecules were compared to the initial CN radical number density, obtained from the laser pulse energy (typical values were ~11 mJ/pulse), and the 266-nm absorption coefficient of ICN (0.009 cm^{-1} $Torr^{-1}$, base e), and assuming a unity quantum yield for CN production. This results in typical values of $[CN]_0 \sim 4.37 \times 10^{13}$ molecule cm^{-3}. Table I shows the resulting yields, assuming conversion of 92% of CN radicals to CH_2OH in reaction (3a). Channel (3.1g) is not directly detected, but any NCO produced in (1g) would be expected to produce N_2O via the NCO+NO reaction.

Although as described above, reaction (3a) is a relatively clean source of CH_2OH radicals, a small (~8%) yield of methoxy (CH_3O) radicals is also produced. Therefore, the following competing reaction must be considered:

$$CH_3O + NO \rightarrow CH_3ONO \quad (3.7a)$$

$$\rightarrow CH_2O + HNO \quad (3.7b)$$

This reaction has a somewhat pressure dependent rate constant, varying from ~$(0.5\text{-}2)\times10^{-11}$ cm^3 $molecule^{-1}$ s^{-1} over the pressure range ~2-100 Torr, with rather small yields of channel 4b of φ_{4b} = 0.15-0.33.[59] Combined with the small yield of (3b), it therefore appears that only very small yields, of approximately 2-3%, of HNO would be produced by this route.

Table 5: Product yields as a fraction of CH_2OH radicals generated.

Product	Fraction of CH_2OH Radicals
HCN	<0.10
HNO	0.11 ± 0.03
HNCO	0.103 ± 0.050
HCNO	<0.02
CO	<0.01
CH_2O	<0.08
N_2O	<0.01

Note: Uncertainties represent one standard deviation.

Deuterated analogs of CH_3OH, CH_3OD and CD_3OH, were used in some experiments to investigate the reaction mechanism. The HNCO signal obtained with CH_3OD was unchanged from that with CH_3OH. Conversely, when CH_3OH was replaced with CD_3OH in the reaction mixture, the HNCO transient signal disappeared and no static signal growth was observed after 100 shots of the excitation laser. These results clearly indicate that the hydrogen atom in HNCO is taken from the alkyl position of CH_2OH. Deuterated analogs were also used in HNO

detection experiments, but due to the small size of the transient signal, the results were inconclusive.

Although we are unable to detect the collisionally stabilized adduct $HOCH_2NO$ from channel (3.1a), the low yields observed for bimolecular product channels (3.1b) and (3.1d), as well as the insignificant yields of other bimolecular channels strongly suggests that adduct formation is in fact the predominate pathway, even at the fairly low total pressures used in this experiment. If true, one would expect that the total rate constant be pressure-dependent. We are not aware of any report of the pressure dependence of reaction (3.1), and our available infrared lasers are not able to detect the CH_2OH radical, but this would clearly be a useful future experiment.

3.4. Conclusions

Reactions of CH_2OH and its partially deuterated analogs were studied by infrared absorption spectroscopy. Small but measurable yields of HNO and HNCO product channels were detected. Although not directly detected, it is likely that collisionally stabilized adduct formation dominates this reaction.

4. CONCLUSIONS

The reactions of CN radicals with small alcohols, and the reactions of hydroxymethyl radicals with nitric oxide were studied by infrared diode laser spectroscopy. The kinetics of the reaction of CN with methanol were found to be fast, and it was found that the methyl hydrogen was preferentially abstracted over the hydroxyl hydrogen with approximately 92% selectivity. The kinetics of the reactions of CN with larger primary alcohols, such as ethanol and n-propanol, were found to be faster than the reaction of CN with methanol. This reaction provides a relatively clean, photolytic pathway to the hydroxymethyl radical, which may be of interest to atmospheric and combustion chemists. The reaction of hydroxymethyl with nitric oxide probably undergoes adduct formation as the major channel, but significant amounts of isocyanic acid and nitroxyl were also detected.

5. REFERENCES

1. Smith, Gregory P.; Golden, David M.; Frenklach, Michael; Moriarty, Nigel W.; Eiteneer, Boris; Goldenberg, Mikhail; Bowman, C. Thomas; Hanson, Ronald K.; Song, Soonho; Gardiner William C., Jr.; Lissianski, Vitali V.; and Qin, Zhiwei. GRI-Mech 3.0. http://www.me.berkeley.edu/gri_mech/ (accessed Jun 8, 2015)

2. Al-Wakeel, Haitham B.; Abdul Karim, Z.A.; Al-Kayiem, Hussain H.; Mat Jamlus, M.H. Soot Reduction Strategy: A Review. *Journal of Applied Sciences*, **2012,** *12*, 2338-2345.

3. Yang, Ruoyan; Gao, Yanshan; Wang, Junya; Wang, Qiang. Layered double hydroxide (LDH) derived catalysts for simultaneous catalytic removal of soot and NO_X. *Dalton Trans.* **2014,** *43*, 10317.

4. Zel'dovich, Y.B. The Oxidation of Nitrogen in Combustion Explosions. *Acta Physicochimica U.S.S.R.* **1946,** *21*, 577–628.

5. Fenimore, C.P. Formation of Nitric Oxide in Premixed Hydrocarbon Flames. *13th Symp. (Int'l) on Combustion* **1971,** 373.

6. Smoot, L. D.; Hill, S. C.; Xu, H. NO_X Control Through Reburning. *Prog. Energy Combust. Sci.* **1998,** *24*, 385-408.

7. Rothman, L. S.; et al. The HITRAN 2012 molecular spectroscopic database. *J. Quant. Spectrosc. Radiat. Transfer*. **2013,** *130*. 4-50.

8. Baulch, D.L.; Cobos, C.J.; Cox, R.A.;Frank, P.; Hayman, G.; Just, Th.; Kerr, J.A.; Murrells, T.; Pilling, M.J.; Troe, J.; Walker, R.W.; Warnatz, J. Evaluated kinetic data for combusion modelling. Supplement I. *J. Phys. Chem. Ref. Data* **1994** *23* 847-1033, and references therein.

9. Anastasi, C.; Hancock, D.U. Reaction of CN radicals with CH_4 and O_2. *J. Chem. Soc., Faraday Trans,* **1988** *84* 9-15.

10. Lichtin, D.A.; Lin M.C. Kinetics of CN radical reactions with selected molecules at room temperature. *Chem. Phys.* **1985** *96* 473-482.

11. Balla, R.J.; Castleton; K.H. Kinetic study of the reactions of cyanyl radical with oxygen and carbon dioxide from 292 to 1500 K using high-temperature photochemistry. *J. Phys. Chem.* **1991** *95* 2344-2351.

12. Sims,I.R.; Queffelec, J.-L.; Travers, D.; Row, B.R.; Herbert, L.B.; Karthauser, J.; Smith, I.W.M. Rate constants for the reactions of CN with hydrocarbons at low and ultra-low temperatures. *Chem. Phys. Lett.* **1993** *211* 461-468.

13. Herbert, L.; Smith, I. W. M.; Spencer-smith, R. D. Rate constants for the elementary reactions between CN radicals and CH_4, C_2H_6, C_2H_4, C_3H_6, and C_2H_2 in the range: 295 ⩽ T/K ⩽ 700. *Int. J. Chem. Kinet.* **1992** *24* 791–802.

14. Yang, D.L.; Yu, T.; Lin, M.C.; Melius, C.F. The reaction of CN with CH_4 and CD_4: an experimental and theoretical study. *Chem. Phys.* **1993** *177* 271-280.

15. Reisler, H.; Mangir, M. ; Wittig, C. The kinetics of free radicals generated by IR laser photolysis. II. Reactions of C_2(X 1Σ+g), C_2(a 3Πu), C_3($\bar{X}$ 1Σ+g) and CN(X 2Σ+) with O2 *Chem. Phys.* **1980** *47* 49-58.

16. Louge, M.Y.; Hanson, R.K. Shock tube study of cyanogen oxidation kinetics *Int. J. Chem. Kinet.* **1984** *16* 231-250.

17. Sims, I.R.; Queffelec, J.-L.; Defrance, A.; Rebrion-Rowe, C.; Travers, D.; Bocherel, P.; Rowe, B.R.; and Smith, I.W.M. Ultralow temperature kinetics of neutral–neutral reactions. The technique and results for the reactions CN+O_2 down to 13 K and CN+NH_3down to 25 K. *J. Chem. Phys.* **1994** *100* 4229.

18. Jensen, R.C.; Walton, D.B.; Coombe, R.D. Rate constants for the reactions of CN radicals with Cl_2, F_2 and O_2. *Chem. Phys. Lett.* **1990** *169* 441-444.

19. Durant, J.L., Jr.; Tully, F.P. Kinetic study of the reaction between CN AND O_2 from 295 to 710 K. *Chem. Phys. Lett.* **1989** *154*, 568-572.

20. Atakan, B.; Jacobs, A.; Wahl, M.; Weller, R.; Wolfrum, J. Kinetic studies of the gas-phase reactions of CN with O_2 and H_2 from 294 to 1000 K. *Chem. Phys. Lett.* **1989** *154* 449-453.

21. Burmeister, M.; Gulati, S.K.; Natarajan, K.; Theilen, K.; Mozzhukin, E.; Roth, P. High temperature rate coefficient for the reaction CN+O_2→NCO+O using different CN-sources. *Symp. (Int.) Combust. (Proc.)* **1989** *22* 1083-1092.

22. Sims, I.R.; Smith, I.W.M. Pressure and temperature dependence of the rate of reaction between CN radicals and NO over the range 99 ⩽*T*/K ⩽ 450. *J. Chem. Soc. Faraday Trans.* **1993** *89* 1-5.

23. You, Y.Y.; Wang, N.S. Rate coefficients of the reactions of CN and NCO with O_2 and NO_2 at 296 K. *J. Chin. Chem. Soc.* **1993** *(Taipei) 40* 337-343.

24. Tsang, W. Chemical kinetic data base for propellant combustion. II. Reactions involving CN, NCO, and HNCO. *J. Phys. Chem. Ref. Data* **1992** *21* 753-791, and references therein.

25. Rim, K.T.; Hershberger, J.F. Temperature dependence of the product branching ratio of the CN + O_2 reaction. *J. Phys. Chem. A.* **1999** *103* 3721-3725.

26. Feng, W.; Hershberger, J.F. Reinvestigation of the Branching Ratio of the CN + O_2 Reaction. *J. Phys. Chem. A* **2009** *113* 3523-3527.

27. Park, J.; Hershberger, J.F. Kinetics and product branching ratios of the CN+NO_2 reaction. *J. Chem. Phys.* **1993** *99* 3488-3493.

28. Park, J.; Hershberger, J.F. Kinetics of the CN + OCS reaction. *Chem. Phys. Lett.* **1998** *295* 89-94.

29. Feng, W.; Hershberger, J.F. Kinetics of the CN + CS_2 and CN + SO_2 Reactions *J. Phys. Chem. A.* **2011** *115* 286-290.

30. Feng, W.; Hershberger, J.F. Kinetics of the CN + HCNO Reaction *J. Phys. Chem. A.* **2006** *110* 12184.

31. Feng, W.; Hershberger, J.F. Product Channels of the CN + HCNO Reaction *J. Phys. Chem. A.* **2012** *116* 10285.

32. Rothman, L. S.; et al. The HITRAN molecular database: Editions of 1991 and 1992. *J. Quant. Spectrosc. Radiat. Transfer.* **1992** *48* 469.

33. Cerny, D.; Bacis, R.; Guelachvili, G.; Roux, F. Extensive analysis of the red system of the CN molecule with a high resolution Fourier Spectrometer. *J. Mol. Spectrosc.* **1978** *73* 154-167.

34. Möllmann, E.; Makib, M.; Winnewissera, A.G.; Winnewissera, B. P.; Quapp, W. High-Temperature Infrared Emission Spectra of $D^{12}C^{14}N$ and $D^{13}C^{14}N$. *J. Mol. Spectrosc.* **2002** *212* 22-31.

35. Hunt, N.; Foster, S.C.; Johns, J.W.C.; McKellar, A.R.W. High-resolution spectroscopy of 16 bands of OCS in the region 1975–2140 cm^{-1} for diode laser calibration. *J. Mol. Spectrosc.* **1985** *111* 42-53.

36. Dóbé, S.; Bérces, T.; Temps, F.; Wagner, H.Gg.; Ziemer, H. Formation of methoxy and hydroxymethyl free radicals in selected elementary reactions. *Symp. Int. Comb. Proc.* **1994** *25* 775-781.

37. Pagsberg, P.; Munk, J.; Anastasi, C.; Simpson, V.J. Reaction of CH_2OH with O_2, NO, and NO_2 at room temperature. *J. Phys. Chem.* **1989,** *93,* 5162-5165.

38. Zhang, J.X.; Li, Z.S.; Liu, J.Y.; Sun, C.C. Theoretical mechanistic study on the radical-molecule reaction of CH_2OH with NO_2. *J. Phys. Chem. A.* **2006,** *110,* 2690- 2697.

39. Schocker, A.; Uetake, M.; Kanno, N.; Koshi, M.; Tonokura, K. J. *Phys. Chem. A.* **2007,** *111,* 6622- 6627.

40. Dóbé, S.; Otting, M.; Temps, F.; Wagner, H.Gg.; Ziemer, H. Fast flow kinetic studies of the reaction $CH_2OH+HCl \rightleftarrows H_3OH+Cl$. The heat of formation of hydroxymethyl. *Ber. Bunsenges. Phys. Chem.* **1993** *97*, 877-884.

41. Dóbé, S.; Bérces, T.; Turanyi, T.; Marta, F.; Grussdorf, J.; Temps, F.; Wagner, H.Gg. Direct kinetic studies of the reactions Br + CH_3OH and CH_2OH + HBr: the heat of formation of CH_2OH. *J. Phys. Chem.* **1996,** *100*, 19864-19873.

42. Seetula, J.A.; Gutman, D. Kinetics of the CH_2OH + HBr and CH_2OH + HI reactions and determination of the heat of formation of CH_2OH. *J. Phys. Chem.* **1992,** *96*, 5401-5405.

43. Jodkowski, J.T.; Rayez, M-T.; Rayez, J-C.; Bérces, T.; Dóbé, S. Theoretical study of the kinetics of the hydrogen abstraction from methanol. 1. Reaction of methanol with fluorine atoms *J. Phys. Chem. A.* **1998** *102* 9219-9229.

44. Jodkowski, J.T.; Rayez, M.-T.; Rayez, J.-C. Theoretical Study of the Kinetics of the Hydrogen Abstraction from Methanol. 3. Reaction of Methanol with Hydrogen Atom, Methyl, and Hydroxyl Radicals. *J. Phys. Chem. A.* **1999** *103* 3750-3765.

45. Tsuboi, T.; Hashimoto, K. Shock Tube Study on Homogeneous Thermal Oxidation of Methanol. *Combust. Flame.* **1981** *42* 61.

46. Tsang, W. Chemical kinetic data base for combustion chemistry. Part 2. Methanol. *J. Phys. Chem. Ref. Data.* **1987** *16* 471.

47. Tsang, W. Chemical kinetic data base for combustion chemistry. Part 3. Propane. *J. Phys. Chem. Ref. Data.* **1988** *17* 887.

48. Tsang, W. Chemical kinetic data base for combustion chemistry. Part 4. Isobutane *J. Phys. Chem. Ref. Data.* **1990** *19* 1-68.

49. Pagsberg, P.; Munk, J.; Sillesen, A.; Anastasi, C. UV spectrum and kinetics of hydroxymethyl radicals. *Chem. Phys. Lett.* **1988** *146* 375.

50. Grotheer, H.-H.; Riekert, G.; Meier, U.; Just, Th. Kinetics of the reactions of CH_2OH radicals with O_2 and HO_2. *Ber. Bunsenges. Phys. Chem.* **1985** *89* 187.

51. Chase, M.W. NIST-JANAF Thermochemical Tables. *J. Phys. Chem. Ref. Data* **1998,** 4th ed.

52. Schuurman, M.S.; Muir, S.R.; Allen, W.D.; Schaefer, H.F., III. Toward subchemical accuracy in computational thermochemistry: Focal point analysis of the heat of formation of NCO and [H,N,C,O] isomers. *J. Chem. Phys.* **2004** *120* 11586-11599.

53. Soto, M.R.; Page, M. Theoretical study of atomic hydrogen + hydroxyimidogen abstraction and addition reactions. *Chem. Phys. Processes Combust.* **1991** *64* 1-4.

54. Dóbé, S.; Bérces, T.; Turányi, T.; Márta, F. Direct Kinetic Studies of the Reactions Br + CH_3OH and CH_2OH + HBr: The Heat of Formation of CH_2OH. *J. Phys. Chem.* **1996** *100* 19864-19873.

55. Fischer, G.; Geith, J.; Klapötke, T.M.; Krumm, B. Synthesis, Properties and Dimerization Study of Isocyanic acid. *Z. Naturforsch.* **2002** *57 b* 19-24.

56. Feng, W.; Hershberger, J.F. Quantification of the 248 nm Photolysis Products of HCNO (Fulminic Acid). *J. Phys. Chem. A* **2014** *118* 829-837.

57. Johns, J.W.C.; McKellar, A.R.W.; Weinberger, E. The infrared spectrum of HNO. *Can. J. Phys.* **1983** *61* 1106-1119.

58. Steiner, D.A.; Polo, S.R.; McCubbin, T.K., Jr. Infrared Spectrum of the Fundamental ν_2 of Isocyanic Acid. *J. Mol. Spectrosc.* **1983** *98* 453-483.

59. Ferretti, E.L.; Rao K. Narahari. Infrared Bands of the HCNO Molecule. *J. Mol. Spectrosc.* **1974** *51* 97-106.

60. Ohmori, K.; Yamasaki, K.; Masui, H. Pressure Dependence of the Rate Constant for the Reaction of CH_3O + NO. *Bull. Chem. Soc. Jpn.* **1993** *66* 51-56.